Hindawi
Complexity
Volume 2020, Article ID 9321928, 17 pages
https://doi.org/10.1155/2020/9321928

Research Article

A Case Study on Designing a Sliding Mode Controller to Stabilize the Stochastic Effect of Noise on Mechanical Structures: Residential Buildings Equipped with ATMD

Aydin Azizi

School of Engineering, Computing and Mathematics, Oxford Brookes University, Wheatley Campus, Oxford OX33 1HX, UK

Correspondence should be addressed to Aydin Azizi; aydin.azizi@brookes.ac.uk

Received 16 April 2019; Accepted 8 October 2019; Published 20 March 2020

Guest Editor: Manuel Zamora

This study aims to stabilize the unwanted fluctuation of buildings as mechanical structures subjected to earth excitation as the noise. In this study, the ground motion is considered as a Wiener process, in which the governing stochastic differential equations have been presented in the form of Ito equation. To stabilize the vibration of the system, the ATMD system is considered and located on the upmost story of the building. A sliding mode controller has been utilized to control the ATMD system, which is a robust controller in the presence of uncertainty. For this purpose, the design of a sliding mode controller for the general dynamic system with Lipschitz nonlinearity and considering the Ito relations has been accomplished. The mentioned design has been implemented considering the presence of the Weiner process and existence of uncertainty in the structure and actuator. Then, the obtained general control law has been generalized to control the ATMD system. The results show that the designed controller is effective to reduce the effect of the unwanted impused vibrations on the building.

1. Introduction

Stochastic factors are one of the inherent aspects of most dynamical systems that occur in different ways such as external force and changes in the inherent parameters of the system. Stochastic Differential Equations (SDE) in financial mathematics and economics have been extensively investigated [1–6]. Also, the effect of stochastic factors in science and mechanical and electronic engineering has been considered [7–20].

Earthquake is an example of a natural phenomenon that influences the dynamics of a structures and building. Dynamic behavior of structures in the presence of earthquakes has been extensively studies in [21–27]. In the mentioned studies, the dynamic behavior of the structures has been investigated under the influence of a particular earthquake. But in this paper, we aim to examine the dynamic behavior of the structure subjected to White Gaussian Noise (WGN) because the density function of its power spectrum is constant at all frequencies. So, unlike the previous studies, a new formulation should be considered.

For this purpose, Itô formulation is considered to solve governing SDE of the structure [28–30]. The studied structure is an 11-story building equipped with an ATMD system at the upmost story. ATMD has been used to reduce unwanted vibrations. This system has been controlled by means of the sliding mode controller. For this reason, the sliding mode controller has been designed for the general and nonlinear Lipschitz dynamic system in the presence of actuator and system uncertainties and based on the Itô theory. Finally, the designed controller has been generalized to control the ATMD system.

The dynamic behavior of the structure in the active and passive mode and considering the uncertainties has been studied. The effect of various controller parameters on the dynamic behavior of the structure has been also investigated. Moreover, the effect of the controlled system and different parameters of the controller on the basin of attraction was

also studied. At the end, the controller's robustness to structural and actuator uncertainty has been studied and the obtained results have been presented.

2. Model Description

The physical and geometrical models of the studied system are presented in this section. The studied model is an 11-story building, the schematic view of which is shown in Figure 1. The mass of each story is denoted by m_i, where i represents the story number. Moreover, the stiffness and damping coefficient for each story are represented by K_i and C_i, respectively. The degree of freedom (DoF) of the system is considered along the horizontal direction, since the ground displacement effects are horizontally applied to the structure. As shown in Figure 1, the displacement of each story is denoted by x_i. Upon ground excitation, each story experiences a vibration and, given that the first mode of vibration is more likely to occur, the largest displacement occurs in the topmost story. To alleviate this deformation caused by earthquakes, the 11^{th} story is equipped with an ATMD system. The mass of this system, its stiffness, and damping coefficient are denoted by m_{12}, K_{12}, and C_{12}. After installation, the DoF of system increases to 12.

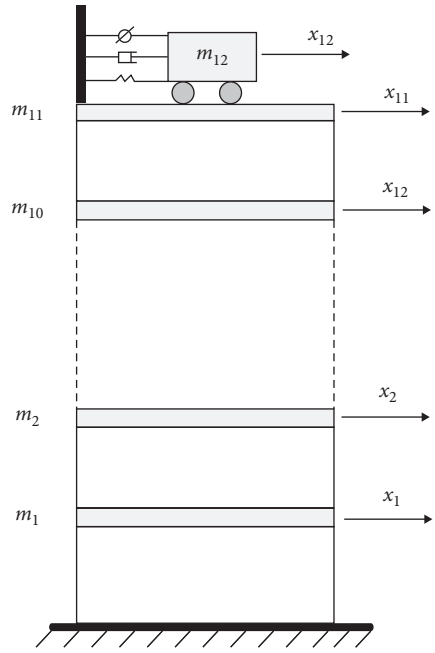

Figure 1: Schematic view of the studied building with ATMD.

The dynamic equation governing the system behavior is presented in the following equation [31]:

$$[M][\ddot{X}] + [C][\dot{X}] + [K][X] = [U] + [D]\left[\ddot{X}_g\right], \tag{1}$$

where $[M]$, $[K]$, and $[C]$ denote mass, stiffness, and damping matrices, respectively. Moreover, $[X] = [x_1, x_2, x_3, \ldots, x_{11}, x_{12}]^T$, $[\dot{X}]$, and $[\ddot{X}]$ represent the structural displacement, velocity, and acceleration, respectively. The term $[U] = [0, 0, \ldots, 0, b(x,t)u, -b(x,t)u]^T$ is the control force vector of the ATMD system responsible for controlling the vibrations of the 11^{th} story. The term $[D][\ddot{x}_g]$ denotes the effects of base excitation on the system, where $\ddot{x}_g$ is the acceleration of base excitations and $[D] = -[m_1, m_2, m_3, \ldots, m_{11}, m_{12}]^T$. The nominal matrix values for $[M]$, $[K]$, and $[C]$ are also presented in the following. However, note that uncertainty will be also considered for these values later in the control design process.

$$[M] = \begin{bmatrix} m_1 & 0 & 0 & 0 & 0 & 0 & 0 & 0 & 0 & 0 & 0 & 0 \\ 0 & m_2 & 0 & 0 & 0 & 0 & 0 & 0 & 0 & 0 & 0 & 0 \\ 0 & 0 & m_3 & 0 & 0 & 0 & 0 & 0 & 0 & 0 & 0 & 0 \\ 0 & 0 & 0 & m_4 & 0 & 0 & 0 & 0 & 0 & 0 & 0 & 0 \\ 0 & 0 & 0 & 0 & m_5 & 0 & 0 & 0 & 0 & 0 & 0 & 0 \\ 0 & 0 & 0 & 0 & 0 & m_6 & 0 & 0 & 0 & 0 & 0 & 0 \\ 0 & 0 & 0 & 0 & 0 & 0 & m_7 & 0 & 0 & 0 & 0 & 0 \\ 0 & 0 & 0 & 0 & 0 & 0 & 0 & m_8 & 0 & 0 & 0 & 0 \\ 0 & 0 & 0 & 0 & 0 & 0 & 0 & 0 & m_9 & 0 & 0 & 0 \\ 0 & 0 & 0 & 0 & 0 & 0 & 0 & 0 & 0 & m_{10} & 0 & 0 \\ 0 & 0 & 0 & 0 & 0 & 0 & 0 & 0 & 0 & 0 & m_{11} & 0 \\ 0 & 0 & 0 & 0 & 0 & 0 & 0 & 0 & 0 & 0 & 0 & m_{12} \end{bmatrix},$$

$$[K] = \begin{bmatrix} k_1+k_2 & -k_2 & 0 & 0 & 0 & 0 & 0 & 0 & 0 & 0 & 0 & 0 \\ -k_2 & k_2+k_3 & -k_3 & 0 & 0 & 0 & 0 & 0 & 0 & 0 & 0 & 0 \\ 0 & -k_3 & k_3+k_4 & -k_4 & 0 & 0 & 0 & 0 & 0 & 0 & 0 & 0 \\ 0 & 0 & -k_4 & k_4+k_5 & -k_5 & 0 & 0 & 0 & 0 & 0 & 0 & 0 \\ 0 & 0 & 0 & -k_5 & k_5+k_6 & -k_6 & 0 & 0 & 0 & 0 & 0 & 0 \\ 0 & 0 & 0 & 0 & -k_6 & k_6+k_7 & -k_7 & 0 & 0 & 0 & 0 & 0 \\ 0 & 0 & 0 & 0 & 0 & -k_7 & k_7+k_8 & -k_8 & 0 & 0 & 0 & 0 \\ 0 & 0 & 0 & 0 & 0 & 0 & -k_8 & k_8+k_9 & -k_9 & 0 & 0 & 0 \\ 0 & 0 & 0 & 0 & 0 & 0 & 0 & -k_9 & k_9+k_{10} & -k_{10} & 0 & 0 \\ 0 & 0 & 0 & 0 & 0 & 0 & 0 & 0 & -k_{10} & k_{10}+k_{11} & -k_{11} & 0 \\ 0 & 0 & 0 & 0 & 0 & 0 & 0 & 0 & 0 & -k_{11} & k_{11}+k_{12} & -k_{12} \\ 0 & 0 & 0 & 0 & 0 & 0 & 0 & 0 & 0 & 0 & -k_{12} & k_{12} \end{bmatrix},$$

$$[C] = \begin{bmatrix} c_1+c_2 & -c_2 & 0 & 0 & 0 & 0 & 0 & 0 & 0 & 0 & 0 & 0 \\ -c_2 & c_2+c_3 & -c_3 & 0 & 0 & 0 & 0 & 0 & 0 & 0 & 0 & 0 \\ 0 & -c_3 & c_3+c_4 & -c_4 & 0 & 0 & 0 & 0 & 0 & 0 & 0 & 0 \\ 0 & 0 & -c_4 & c_4+c_5 & -c_5 & 0 & 0 & 0 & 0 & 0 & 0 & 0 \\ 0 & 0 & 0 & -c_5 & c_5+c_6 & -c_6 & 0 & 0 & 0 & 0 & 0 & 0 \\ 0 & 0 & 0 & 0 & -c_6 & c_6+c_7 & -c_7 & 0 & 0 & 0 & 0 & 0 \\ 0 & 0 & 0 & 0 & 0 & -c_7 & c_7+c_8 & -c_8 & 0 & 0 & 0 & 0 \\ 0 & 0 & 0 & 0 & 0 & 0 & -c_8 & c_8+c_9 & -c_9 & 0 & 0 & 0 \\ 0 & 0 & 0 & 0 & 0 & 0 & 0 & -c_9 & c_9+c_{10} & -c_{10} & 0 & 0 \\ 0 & 0 & 0 & 0 & 0 & 0 & 0 & 0 & -c_{10} & c_{10}+c_{11} & -c_{11} & 0 \\ 0 & 0 & 0 & 0 & 0 & 0 & 0 & 0 & 0 & -c_{11} & c_{11}+c_{12} & -c_{12} \\ 0 & 0 & 0 & 0 & 0 & 0 & 0 & 0 & 0 & 0 & -c_{12} & c_{12} \end{bmatrix}. \quad (2)$$

3. Mathematical Modeling

Without loss of generality, the controller is initially designed for a general system, after which it is applied to the studied structural control.

Consider the mathematical model presented in the following equation:

$$\begin{cases} \dot{x}_1 = x_2, \\ \dot{x}_2 = f(x,t) + b(x,t)u + h(x,t)\dot{v}, \end{cases} \quad (3)$$

where $f(x,t)$, $b(x,t)$, and $h(x,t)$ represent continuous functions satisfying the Lipschitz condition. In this case, u, v, and $\dot{v} = \mathrm{d}v/\mathrm{d}t$ indicate the control force, standard Wiener process, and white Gaussian noise, respectively. The objective of the controller design is for the x_1 to track x_d. To this end, the dynamic error of $e = x_1 - x_d$ should be defined. However, since x_d is considered zero in structural control, the error is defined as $e = x_1$ and the corresponding dynamic error is defined as follows:

$$\begin{cases} \dot{e}_1 = x_2 - \dot{x}_d, \\ \dot{e}_2 = f(x,t) + b(x,t)u + h(x,t)\dot{v} - \ddot{x}_d. \end{cases} \quad (4)$$

The Lyapunov function is considered as $V = 1/2E(s^2)$. From a mathematical viewpoint and based on Ito's theory, equation (4) can be reformulated in the form of a differential equation as follows:

$$\begin{cases} \mathrm{d}e_1 = [x_2 - \dot{x}_d]\mathrm{d}t, \\ \mathrm{d}e_2 = [f(x,t) + b(x,t)u - \ddot{x}_d]\mathrm{d}t + h(x,t)\mathrm{d}v, \\ \ddot{x}_d = 0. \end{cases} \quad (5)$$

Given that $x_d = \dot{x}_d = \ddot{x}_d = 0$, the abovementioned equation is presented as follows for simplification purposes:

$$\begin{cases} \mathrm{d}e_1 = [x_2]\mathrm{d}t, \\ \mathrm{d}e_2 = [f(x,t) + b(x,t)u]\mathrm{d}t + h(x,t)\mathrm{d}v. \end{cases} \quad (6)$$

The abovementioned equation represents an Itô SDE used instead of equation (4) and considering the Wiener process. The terms $f(x,t) + b(x,t)u$ and $h(x,t)$ represent the drift function and diffusion, respectively [28, 29].

The sliding surface was considered as $s = e_2 + \lambda e_1$ in the design of the sliding mode controller, from which $\dot{s} = \dot{e}_2 + \lambda e_2$ and $\mathrm{d}s = \mathrm{d}e_2 + \lambda e_2 \mathrm{d}t$ can be derived. In the final form and according to equation (4), the ds equation can be rewritten to obtain equation (5):

$$\mathrm{d}s = [f(x,t) + b(x,t)u + \lambda e_2]\mathrm{d}t + h(x,t)\mathrm{d}v. \quad (7)$$

Assuming $y = g(x,t)$ and employing Itô 's differentiation formula for dy, we have [28, 29]

$$y = g(x,t),$$
$$\mathrm{d}y = \frac{\partial g}{\partial t}\mathrm{d}t + \frac{\partial g}{\partial x}\mathrm{d}x + \frac{1}{2}\frac{\partial^2 g}{\partial x^2}(\mathrm{d}x)^2. \tag{8}$$

Based on Ito's formula, differentiating s^2 produces $\mathrm{d}s^2 = 2s\mathrm{d}s + \mathrm{d}s\mathrm{d}s$. Therefore, the $\mathrm{d}V$ value emerges as follows:

$$\mathrm{d}V = E\Big(s\{[f(x,t) + b(x,t)u + \lambda e_2]\mathrm{d}t + h(x,t)\mathrm{d}v\} + \frac{1}{2}\{[f(x,t) + b(x,t)u + \lambda e_2]\mathrm{d}t + h(x,t)\mathrm{d}v\}^2\Big). \tag{9}$$

By including the following relations proposed by [32, 33] in the calculations,

$$\begin{aligned}\mathrm{d}t \cdot \mathrm{d}t &= 0,\\ \mathrm{d}t \cdot \mathrm{d}v &= 0,\\ \mathrm{d}v \cdot \mathrm{d}v &= \mathrm{d}t.\end{aligned} \tag{10}$$

And also considering the properties of the Wiener process [28],

$$\begin{aligned}E[h(x,t)\mathrm{d}v] &= 0,\\ E[h(x,t)\mathrm{d}v]^2 &= h^2(x,t)\mathrm{d}t.\end{aligned} \tag{11}$$

According to equations (10) and (11), the expected value of $\mathrm{d}V$ is determined as follows:

$$\mathrm{d}V = E\Big(s\{[f(x,t) + b(x,t)u + \lambda e_2]\mathrm{d}t\} + \frac{1}{2}h^2(x,t)\mathrm{d}t\Big). \tag{12}$$

Dividing the abovementioned relation by $\mathrm{d}t$, $\dot{V}$ is obtained as follows:

$$\dot{V} = E\big(s[f(x,t) + b(x,t)u + \lambda e_2]\big) + \frac{1}{2}E\big\{h^2(x,t)\big\}. \tag{13}$$

The stability condition for the sliding mode controller is defined as $\dot{V} < 0$ based on the Lyapunov second method for stability [34]. Assuming the systems involve no uncertainty, the controller stability is only guaranteed by considering $f(x,t) + b(x,t)u + \lambda e_2 = -\theta s$, limiting the region of attraction associated with the sliding surface. However, given the presence of uncertainty in most of dynamical systems, the system uncertainties are included in the controller design equations in the following part.

The structural and actuator uncertainties have been considered in the controller model in this study. To this end, some of the inequalities associated with the $f(x,t)$ and $b(x,t)$ functions along with their nominal values should be taken into account.

Assuming $\widehat{f}(x,t)$ as the nominal values for $f(x,t)$ and $F(x,t)$ is a positive function expressed as follows:

$$\left|f(x,t) - \widehat{f}(x,t)\right| \le F(x,t). \tag{14}$$

As a result, the following equations hold true:

$$\begin{aligned}\left|sf(x,t) - s\widehat{f}(x,t)\right| &\le |s|F(x,t),\\ sf(x,t) &\le s\widehat{f}(x,t) + |s|F(x,t).\end{aligned} \tag{15}$$

If $b(x,t)$ is defined as

$$0 < b_0 < b(x,t) < b_M, \tag{16}$$

where b_0 and b_M are positive values representing the upper and lower bounds of the $b(x,t)$ function, the following equations are necessary for the controller design:

$$|s|F(x,t) \le |s|\frac{b(x,t)}{b_0}F(x,t), \tag{17}$$

$$\begin{aligned}s\lambda e_2 &= s\lambda\frac{b}{b_0}e_2 + s\lambda e_2\left(1 - \frac{b}{b_0}\right),\\ s\lambda e_2 &\le s\lambda\frac{b}{b_0}e_2 + |s|\lambda|e_2|b\left(\frac{1}{b_0} - \frac{1}{b}\right),\\ \text{attention to} \longrightarrow |s|\lambda|e_2|b\left(\frac{1}{b_0} - \frac{1}{b}\right) &\le |s|\lambda|e_2|b\left(\frac{1}{b_0} - \frac{1}{b_M}\right),\end{aligned}$$

So,

$$s\lambda e_2 \le s\lambda\frac{b}{b_0}e_2 + |s|\lambda|e_2|b\left(\frac{1}{b_0} - \frac{1}{b_M}\right), \tag{18}$$

$$\begin{aligned}s\widehat{f}(x,t) &= s\frac{b}{b_0}\widehat{f}(x,t) + s\widehat{f}(x,t)\left(1 - \frac{b}{b_0}\right),\\ s\widehat{f}(x,t) &\le s\frac{b}{b_0}\widehat{f}(x,t) + |s|\left|\widehat{f}(x,t)\right|b\left(\frac{1}{b_0} - \frac{1}{b}\right),\\ \text{attention to} \longrightarrow |s|\left|\widehat{f}(x,t)\right|b\left(\frac{1}{b_0} - \frac{1}{b}\right) &\le |s|\left|\widehat{f}(x,t)\right|b\left(\frac{1}{b_0} - \frac{1}{b_M}\right),\end{aligned}$$

So,

$$s\widehat{f}(x,t) \le s\frac{b}{b_0}\widehat{f}(x,t) + |s|\left|\widehat{f}(x,t)\right|b\left(\frac{1}{b_0} - \frac{1}{b_M}\right). \tag{19}$$

The following inequality holds true considering equations (15), (17), and (19):

$$sf(x,t) \le s\frac{b}{b_0}\widehat{f}(x,t) + |s|\left|\widehat{f}(x,t)\right|b\left(\frac{1}{b_0} - \frac{1}{b_M}\right) + |s|\frac{b(x,t)}{b_0}F(x,t). \tag{20}$$

Equation (21) also holds true considering equations (18) and (20):

$$\dot{V} \le s\lambda \frac{b}{b_0} e_2 + |s|\lambda |e_2| b\left(\frac{1}{b_0} - \frac{1}{b_M}\right) + s\frac{b}{b_0}\widehat{f}(x,t) + |s|\left|\widehat{f}(x,t)\right| b\left(\frac{1}{b_0} - \frac{1}{b_M}\right) + |s|\frac{b}{b_0}F(x,t) + sb(x,t)u + \frac{1}{2}h^2(x,t),$$

$$\dot{V} \le s\frac{b}{b_0}\left[\lambda e_2 + \widehat{f}(x,t)\right] + sb(x,t)u + |s|b\left(\frac{1}{b_0} - \frac{1}{b_M}\right)\left[\lambda|e_2| + \left|\widehat{f}(x,t)\right|\right] + |s|\frac{b}{b_0}F(x,t) + \frac{1}{2}h^2(x,t). \tag{21}$$

By defining u as follows, the relation $\dot{V} \le -\theta E[s^2] + (1/2)E[h^2(x,t)]$ holds true:

$$u = -\frac{1}{b_0}\left[\lambda e_2 + \widehat{f}(x,t) + \theta \times (s)\right] - \text{sign}(s)[\eta + \psi], \tag{22}$$

where η represents a positive value and $\psi(x,t) = ((1/b_0) - (1/b_M))[\lambda|e_2| + |\widehat{f}(x,t)|] + (1/b_0)F(x,t)$. In fact, $u = u_1 + u_2$, where u_1 and u_2, which are obtained as follows, cause the nominal and uncertainty terms to be negative definite, respectively:

$$\begin{aligned} u &= u_1 + u_2, \\ \lambda\frac{1}{b_0}e_2 + \frac{1}{b_0}\widehat{f}(x,t) + u_1 &= -\frac{\theta}{b_0}s, \\ u_1 &= -\frac{1}{b_0}\left[\lambda e_2 + \widehat{f}(x,t) + \theta \times (s)\right], \\ sb(x,t)u_2 + |s|b(x,t)\left\{\left(\frac{1}{b_0} - \frac{1}{b_M}\right)\left[\lambda|e_2| + \left|\widehat{f}(x,t)\right|\right] + \frac{1}{b_0}F(x,t)\right\} &= -\eta b(x,t)|s|, \\ su_2 + |s|\left\{\left(\frac{1}{b_0} - \frac{1}{b_M}\right)\left[\lambda|e_2| + \left|\widehat{f}(x,t)\right|\right] + \frac{1}{b_0}F(x,t)\right\} &= -\eta|s|, \\ \psi(x,t) &= \left(\frac{1}{b_0} - \frac{1}{b_M}\right)\left[\lambda|e_2| + |\widehat{f}(x,t)|\right] + \frac{1}{b_0}F(x,t), \\ su_2 &= -\eta|s| - |s|\psi, \\ su_2 &= -|s|(\eta + \psi), \\ u_2 &= -\text{sign}(s)[\eta + \psi]. \end{aligned} \tag{23}$$

Theory. assume Δ as the following set:

$$\Delta = \left\{ s \in R \,\middle|\, E\left[s^2\right] \le \frac{H^2}{\theta} \right\}, \tag{24}$$

where θ is a positive value. In fact, $\dot{V} \le -\theta E[s^2] + (1/2)E[h^2(x,t)]$ represents the attraction set for the trajectory $s(t)$. Assuming at $t = 0$, the trajectory $s(t)$ lies outside the attraction set, i.e., $E[s^2(t=0)] > H^2/2\theta$, we obtain

$$\dot{V} \le -\theta E\left[s^2(t=0)\right] + \frac{1}{2}E\left[h^2(x,t)\right] < 0, \tag{25}$$

which indicates a declining rate for V as it tends to enter the Δ set and ultimately remains in this region.

If it is located in the domain of s for the moment $t = 0$, it will continue to be in this area.

The designed sliding mode controller is then applied to the system, as shown in Figure 1, based on the above-mentioned equations. The equation governing the dynamic behavior of the 11th story is expressed as follows:

$$\begin{cases} \dot{x}_1 = x_2, \\ \dot{x}_2 = -\frac{1}{M_{11}}\left[(K_{11} + K_{12})x_{11} + (C_{11} + C_{12})\dot{x}_{11} - K_{11}x_{10} - K_{12}x_{12} - C_{11}\dot{x}_{10} - C_{12}\dot{x}_{12}\right] - \ddot{x}_g + \frac{b(x,t)}{M_{11}}u. \end{cases} \tag{26}$$

The $f(x,t)$ for this equation is defined as follows:

$$f(x,t) = -\frac{1}{\widehat{M}_{11} + \Delta M_{11}}\Big[\big(\widehat{K}_{11} + \Delta K_{11} + \widehat{K}_{12} + \Delta K_{12}\big)x_{11} + \big(\widehat{C}_{11} + \Delta C_{11} + \widehat{C}_{12} + \Delta C_{12}\big)\dot{x}_{11} - \big(\widehat{K}_{11} + \Delta K_{11}\big)x_{10} - \big(\widehat{K}_{12} + \Delta K_{12}\big)x_{12} - \big(\widehat{C}_{11} + \Delta C_{11}\big)\dot{x}_{10} - \big(\widehat{C}_{12} + \Delta C_{12}\big)\dot{x}_{12}\Big], \tag{27}$$

where $\widehat{M}_{11}$, $\widehat{K}_{11}$, $\widehat{K}_{12}$, $\widehat{C}_{11}$, and $\widehat{C}_{12}$ denote nominal values and ΔM_{11}, ΔK_{11}, ΔK_{12}, ΔC_{11}, and ΔC_{12} represent the maximum value for the respective uncertainty term.

In this case, $F(x,t)$ is defined as follows:

$$F(x,t) = \frac{1}{\widehat{M}_{11} - \left|\Delta\widehat{M}_{11}\right|}\Big[\big(\left|\Delta\widehat{K}_{11}\right| + \left|\Delta\widehat{K}_{12}\right|\big)\left|x_{11}\right| + \Big(\left|\Delta\widehat{C}_{11}\right| + \left|\Delta\widehat{C}_{12}\right|\Big)\left|\dot{x}_{11}\right| + \left|\Delta\widehat{K}_{11}\right|\left|x_{10}\right| + \left|\Delta\widehat{K}_{12}\right|\left|x_{12}\right| + \left|\Delta\widehat{C}_{11}\right|\left|\dot{x}_{10}\right| + \left|\Delta\widehat{C}_{12}\right|\left|\dot{x}_{12}\right|\Big]. \tag{28}$$

Moreover, $b(x,t)$ is assumed as $b(x,t) = (1+\alpha\sin t)/M_{21}$ in this case, meaning that the system's actuator includes the uncertainty $(1+\alpha\sin t)$. Under these conditions, b_0 and b_M are expressed as follows:

$$b_0 = \frac{1-\alpha}{\widehat{M}_{21} + \left|\Delta\widehat{M}_{21}\right|}, \qquad b_M = \frac{1+\alpha}{\widehat{M}_{21} - \left|\Delta\widehat{M}_{21}\right|}. \tag{29}$$

Finally, the term associated with the control force u is conveniently determined using equation (22).

4. Results and Discussion

In this section, the obtained results will be presented and the control of horizontal displacement of the 11-story building will be discussed. Given that the first vibrational mode of the building is easily excited, the largest displacement in this mode is experienced by the topmost story. Therefore, vibration analysis is conducted on the 11th story. The physical and geometrical specifications of the studied building are given in Table 1. In the first scenario, the uncertainty was assumed as $\Delta M_i = 0.01M_i$, $\Delta K_i = 0.01K_i$, $\Delta C_i = 0.01C_i$, and $\alpha = 0$. The resulting horizontal displacement for story 11 is demonstrated in Figure 2 for both active and passive cases. As shown in this figure, the vibrational amplitude of the controlled system is considerably smaller than that of the uncontrolled system.

The variations of the control force u with respect to time are demonstrated in Figure 3. As shown, the chattering phenomenon is apparent within some time intervals. Chattering is mainly caused by the term $\text{sign}(s)$ in the control force relation. In fact, the discontinuity and undifferentiability of this function at point $s = 0$ is responsible for the chattering phenomenon. The chattering around the zero point is highly harmful, since, in addition to the force magnitude, its sign also changes. However, at nonzero points, the chattering only causes a decrease or increase in the force magnitude. In our case, as shown, chattering occurs at nonzero points.

To resolve the chattering problem and satisfy the continuity and Lipschitz condition, the term $\tanh(s)/\varepsilon$ was used as an approximation of the $\text{sign}(s)$ function for the function

Table 1: The physical and geometrical specifications of the studied building.

Properties	Values
$M_1, M_2, \ldots, M_{11}$	255×10^3 kg
M_{12}	77×10^3 kg
$K_1, K_2, \ldots, K_{11}$	25×10^6 N/m
K_{12}	205×10^3 N/m
$C_1, C_2, \ldots, C_{11}$	216×10^3 Ns/m
C_{12}	438×10^3 Ns/m

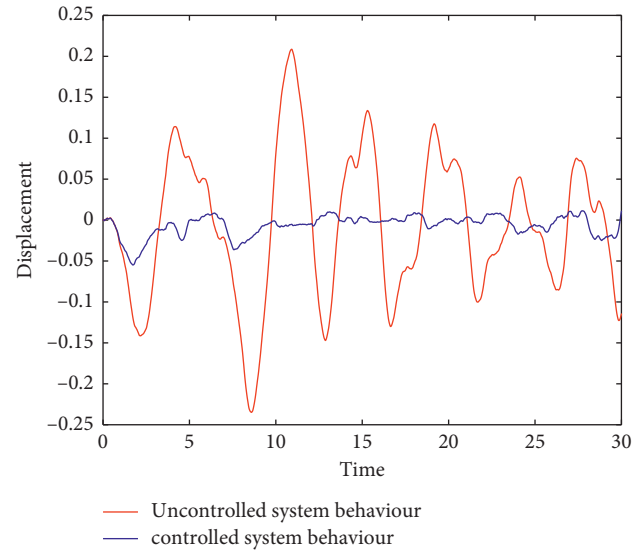

Figure 2: The resulting horizontal displacement for 11th story controlled and uncontrolled cases.

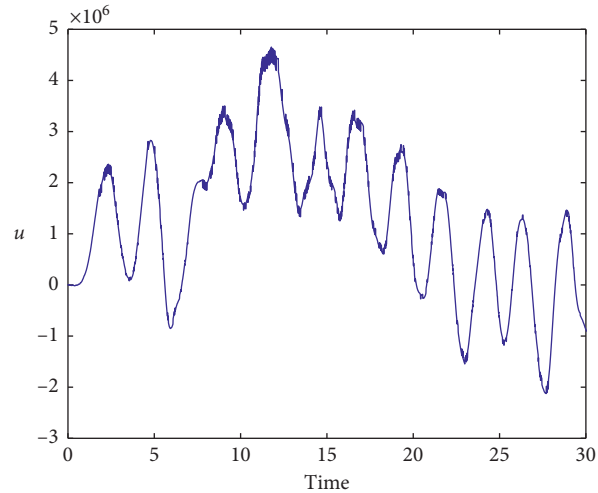

Figure 3: Variation of control parameter u for Figure 2.

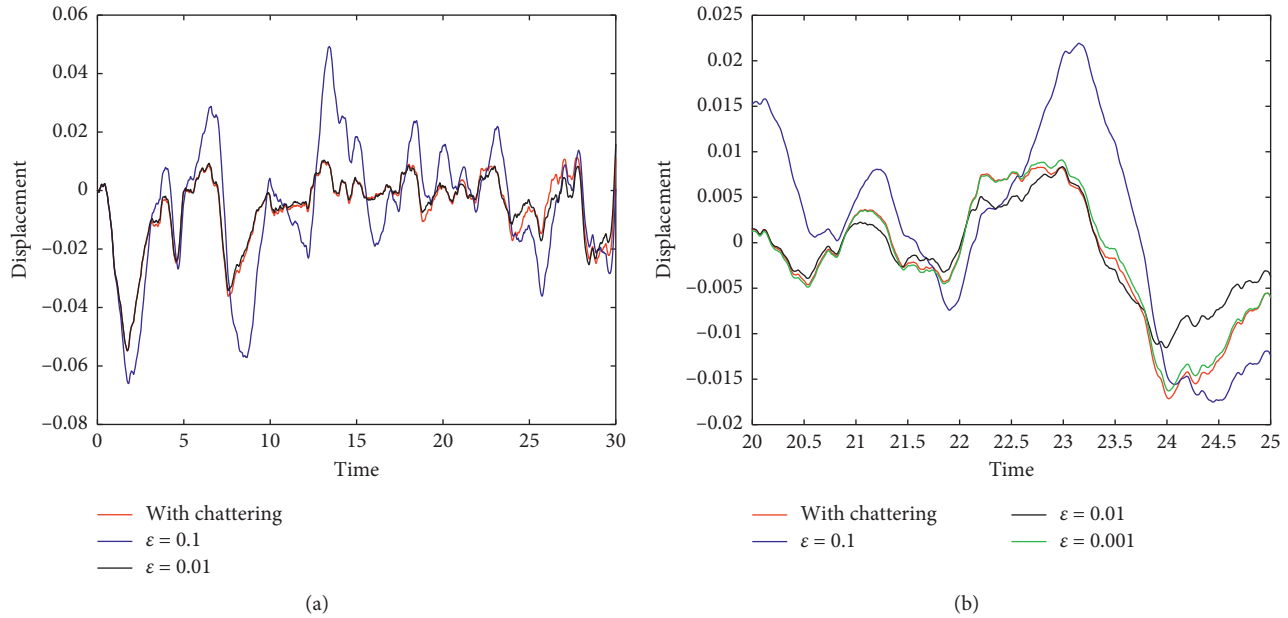

Figure 4: (a) Controlled system behavior for different magnitudes of ε. (b) Detailed view of Figure 4(a).

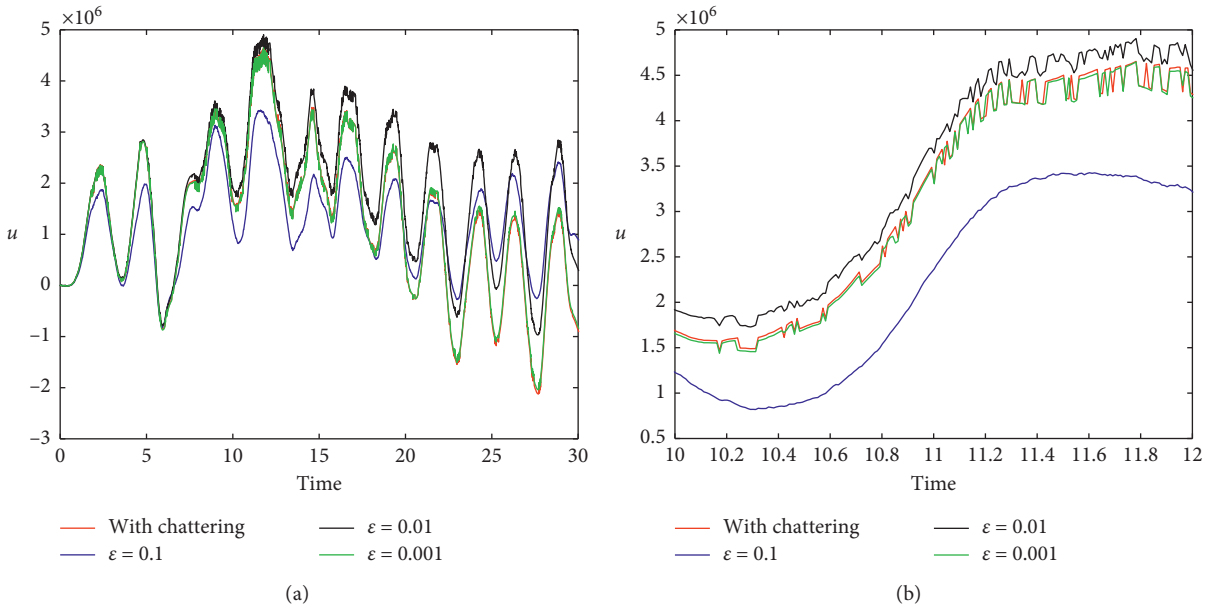

Figure 5: (a) The variations of force u corresponding to Figure 4 for different ε. (b) Detailed view of Figure 5(a).

$b(x,t)u$, where the continuity and differentiability conditions are satisfied at point $s = 0$. The diagram of horizontal displacements for different ε values is demonstrated in Figure 4. As shown, the displacement amplitude is increased by increasing ε. However, this increase is negligible compared to the displacement of the uncontrolled system.

The variations of force u corresponding to Figure 4 for different ε values are shown in Figure 5. As indicated, the amplitude of force u at $\varepsilon = 0.1$ is smaller compared to other ε values. Moreover, the chattering phenomenon is also fully resolved in this case, while it is still observed at other cases, for example, $\varepsilon = 0.001$. As shown in Figures 4 and 5, the vibrational amplitudes for both $\text{sign}(s)$ and $\tanh(s/0.001)$ functions are consistent, which is due to the accurate approximation of the $\text{sign}(s)$ function by $\tanh(s/0.001)$.

Moreover, the phase diagram for the 11$^{\text{th}}$ story is also demonstrated in Figure 6 for different cases. As shown, by increasing ε, the region of attraction is also extended. This region was almost similar for both $\text{sign}(s)$ and $\tanh(s/0.001)$ functions.

The effect of $h(x,t)$ on the dynamic behavior of the structure and the region of attraction is discussed in this part. The vibrational amplitude of the uncontrolled system for different $h(x,t)$ values is shown in Figure 7. As

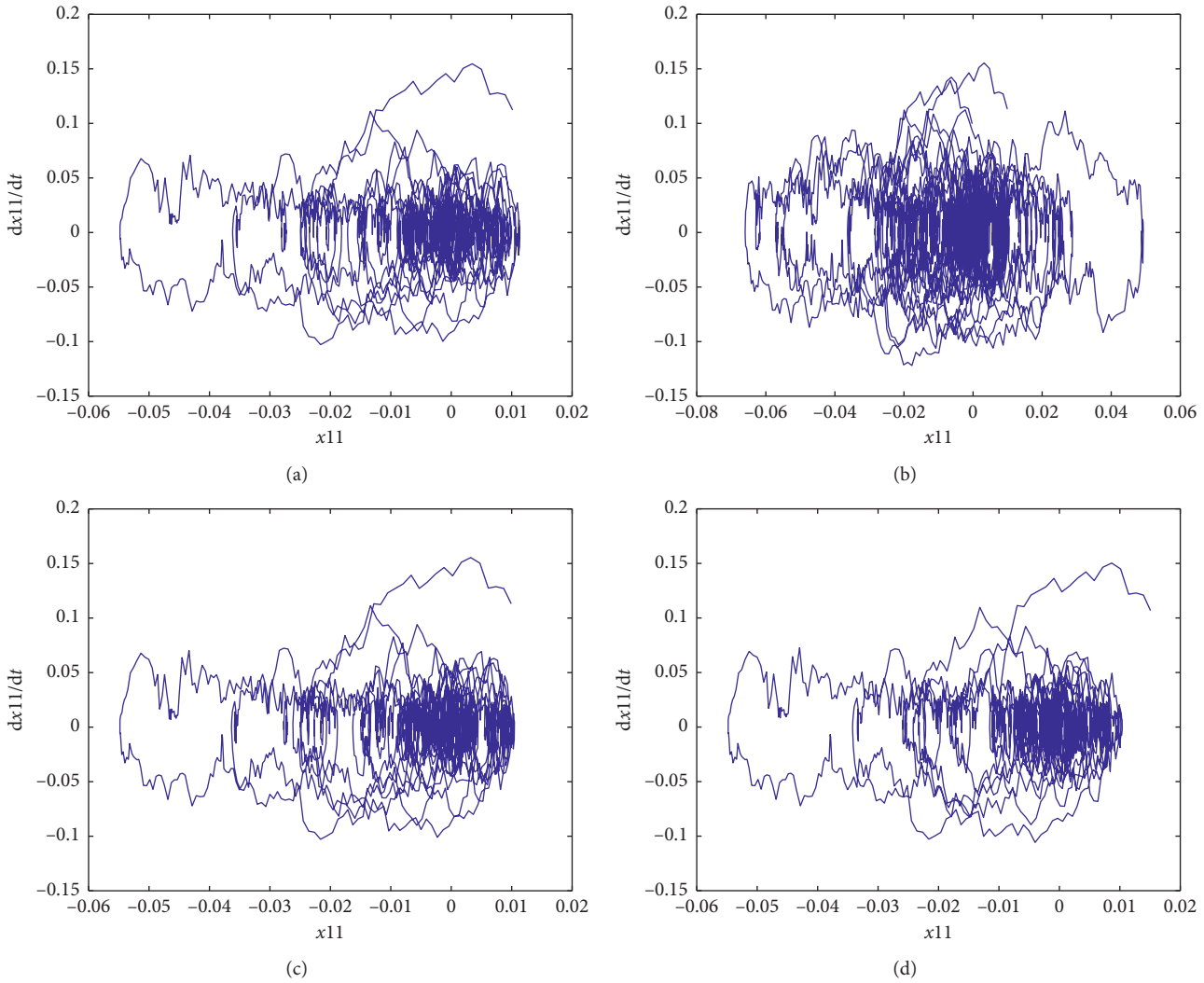

Figure 6: Phase portrait of horizontal displacement of 11th story considering functions sign(s) and tanh(s/ε). (a) sign(s). (b) $\varepsilon = 0.1$. (c). $\varepsilon = 0.01$. (d) $\varepsilon = 0.001$.

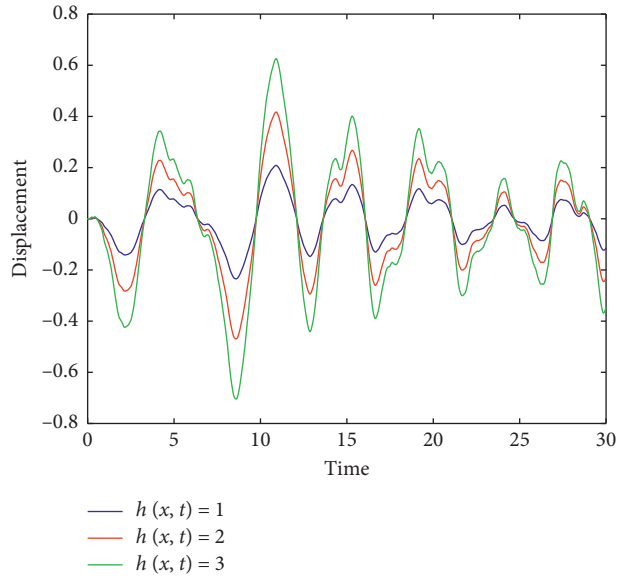

Figure 7: Vibrational behavior of 11th story in the passive mode and for different magnitudes of $h(x,t)$.

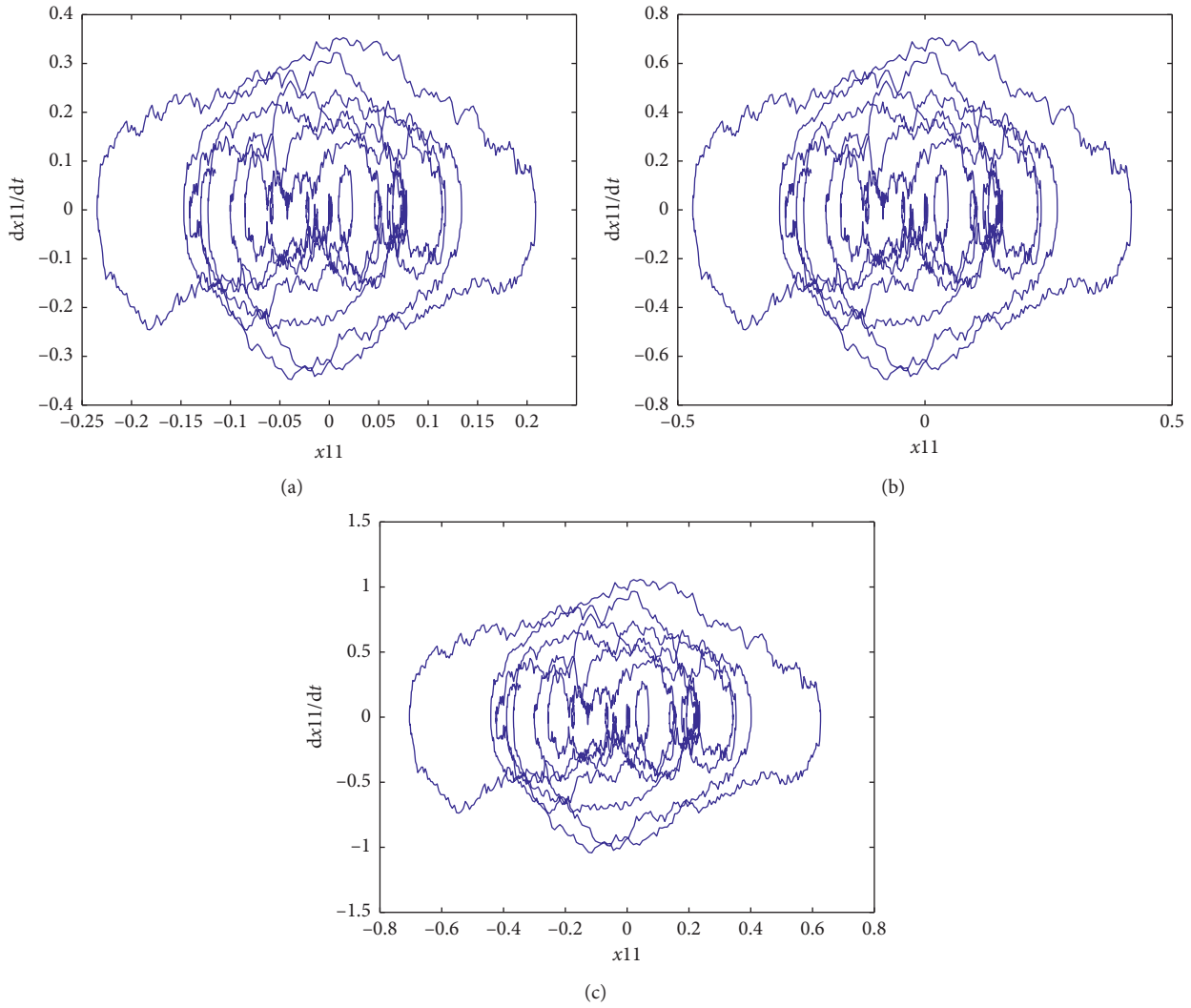

Figure 8: Phase portrait of horizontal displacement of 11th story for passive case and different values of $h(x,t)$. (a) $h(x,t) = 1$. (b) $h(x,t) = 2$. (c) $h(x,t) = 3$.

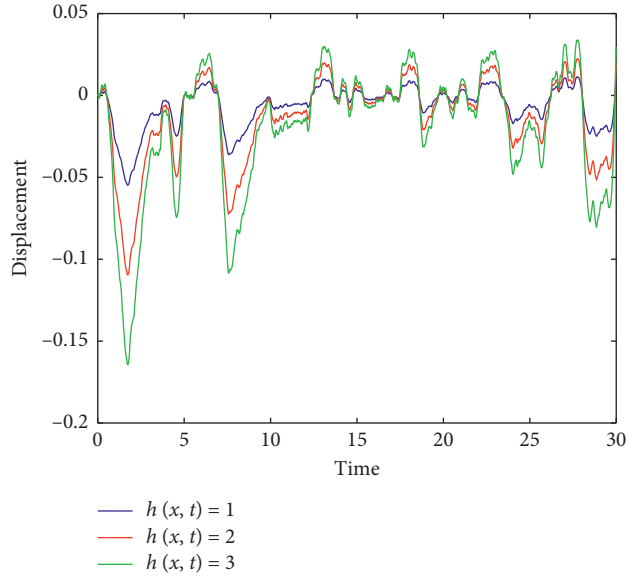

Figure 9: The horizontal displacement of 11th story for the controlled case and for different values of $h(x,t)$.

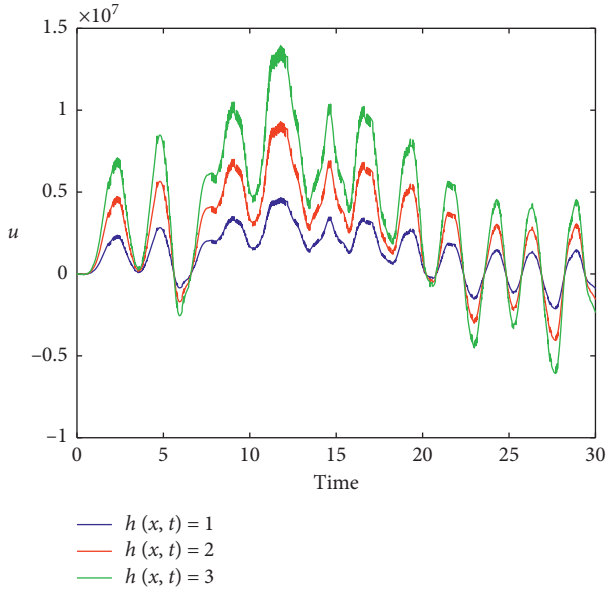

Figure 10: The force variations corresponding to Figure 9.

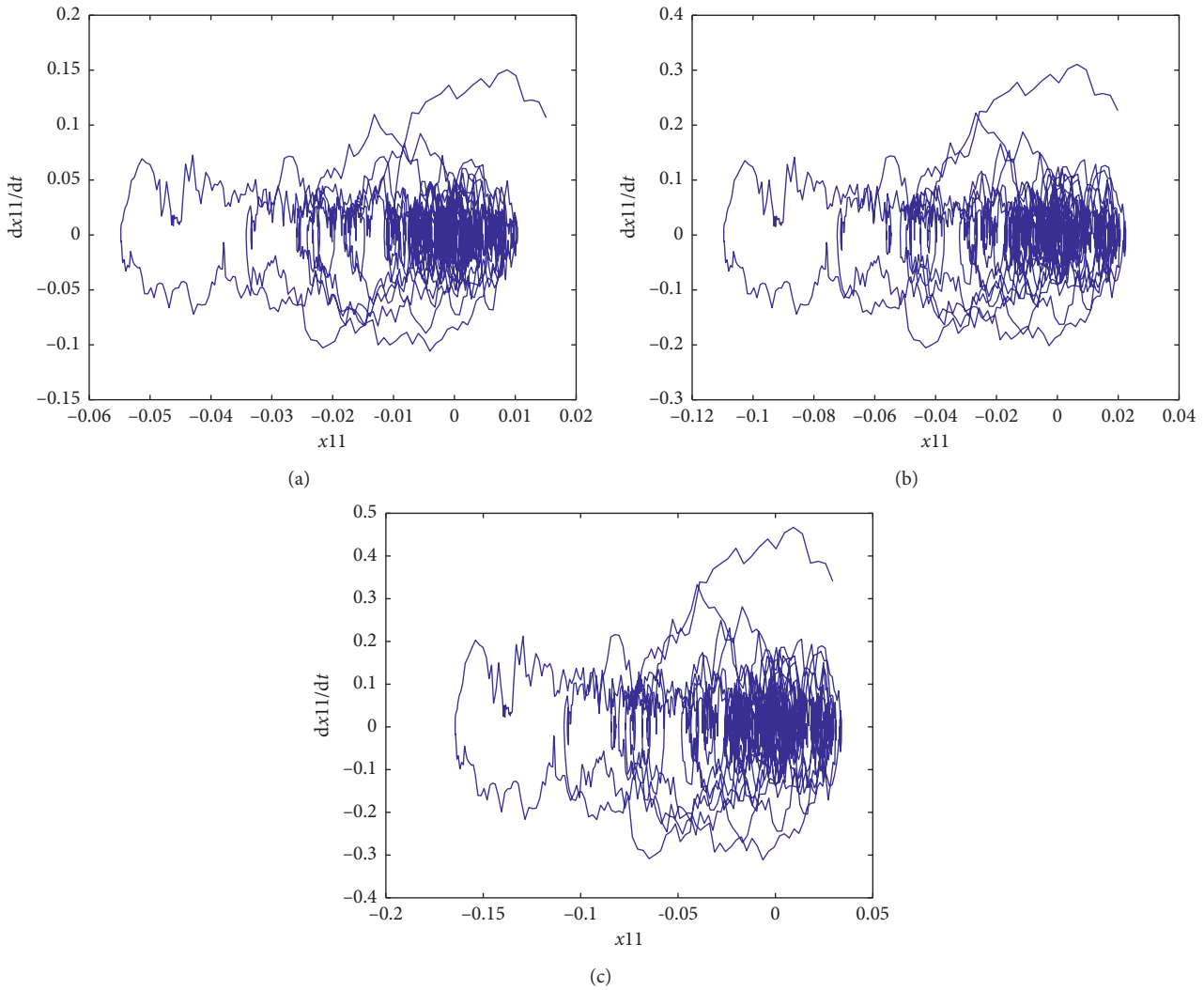

Figure 11: Phase portrait of 11th story for the controlled case and different $h(x,t)$. (a) $h(x,t) = 1$. (b) $h(x,t) = 2$. (c) $h(x,t) = 3$.

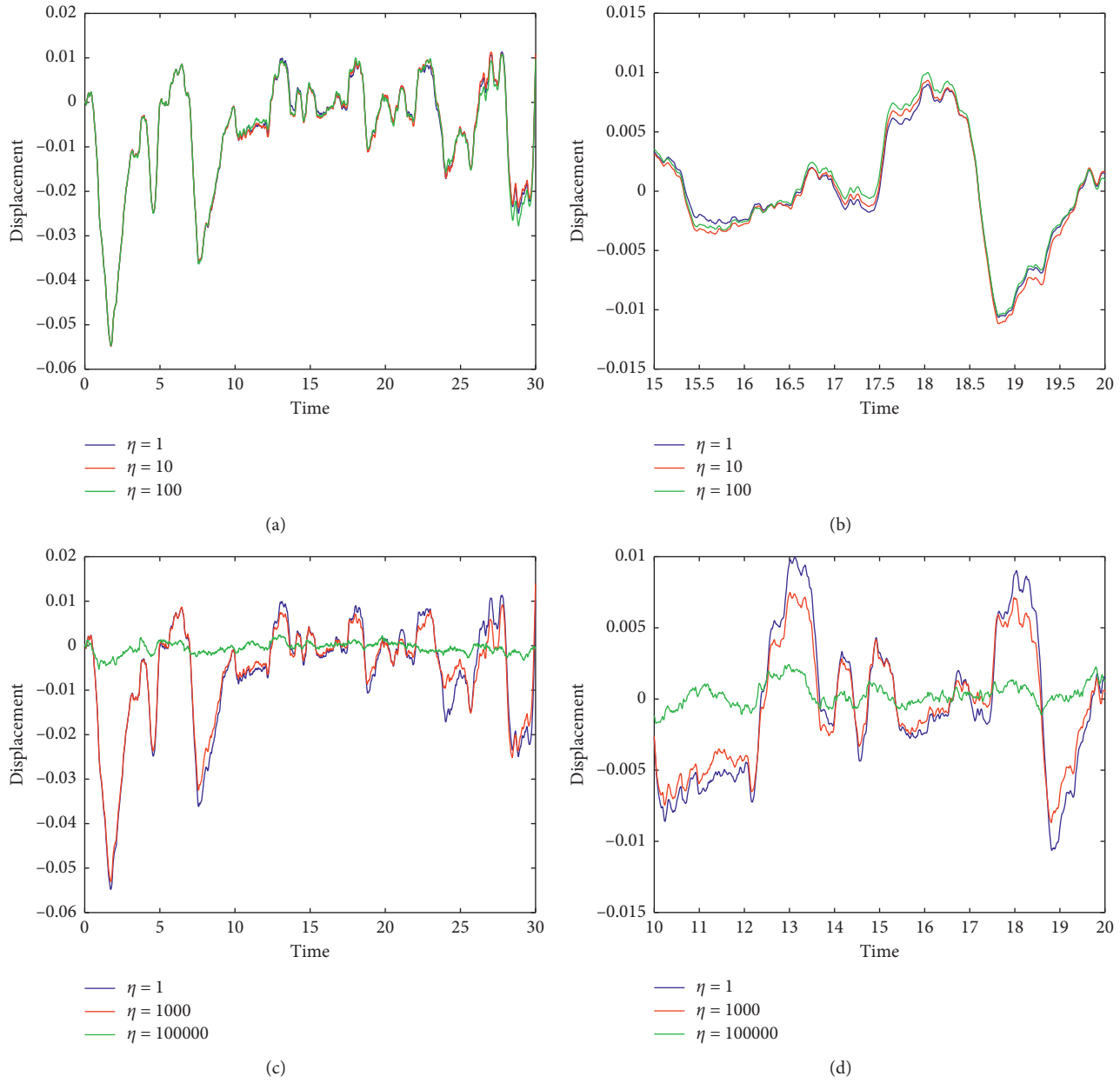

FIGURE 12: The variations in horizontal displacement for different values of η and $\lambda = 1$. (a) The variations in horizontal displacement for $\eta = 1$, $\eta = 10$, and $\eta = 100$ and $\lambda = 1$. (b) Detailed view of Figure 12(a). (c) The variations in horizontal displacement for $\eta = 1$, $\eta = 1000$, and $\eta = 100000$ and $\lambda = 1$. (d) Detailed view of Figure 12(c).

demonstrated, the displacement amplitude is linearly increased by increasing $h(x,t)$.

Also, the attraction domain for the mentioned figure is presented in Figure 8. As is clear from this figure, the domain of attraction set is extended with increasing $h(x,t)$.

The horizontal displacement for the controlled case is demonstrated in Figure 9 with respect to different $h(x,t)$ values. As shown, by increasing $h(x,t)$, the vibrational amplitude is also increased, but its value is substantially smaller compared to the uncontrolled case. The force variations corresponding to Figure 9 is demonstrated in the diagram of Figure 10. As shown, the amplitude of force variations also experiences an increase as $h(x,t)$ increases.

Moreover, the region of attraction corresponding to Figure 9 is demonstrated in Figure 11. As shown, similar to the uncontrolled case, the region of attraction increases by increasing $h(x,t)$.

The effects of η and λ on the behavior of a controlled system is discussed in this section. The variations in horizontal displacement of the system are demonstrated in Figure 12 for different η values. As shown, for η values lower than 1000, increasing the η values is not significantly effective, but increasing this parameter to 100,000 causes the

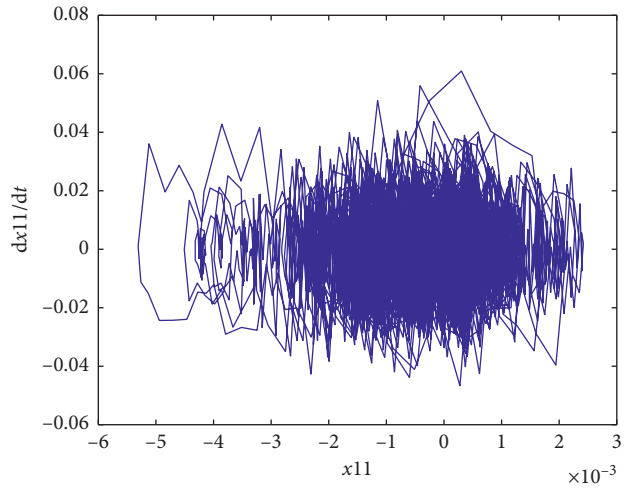

Figure 13: Phase portrait and basin of the attraction set for the active case with $\eta = 100000$ and $\lambda = 1$.

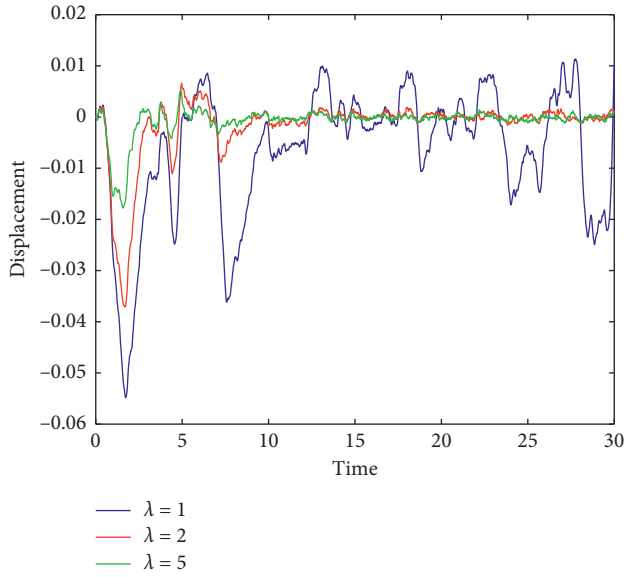

Figure 14: The horizontal displacement amplitude of the active system for different λ values and $\eta = 1$.

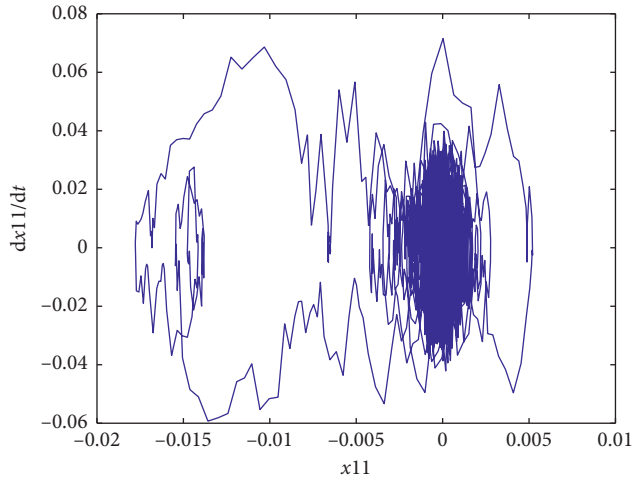

Figure 15: The phase portrait of 11th story for the active system considering $\eta = 1$ and $\lambda = 5$.

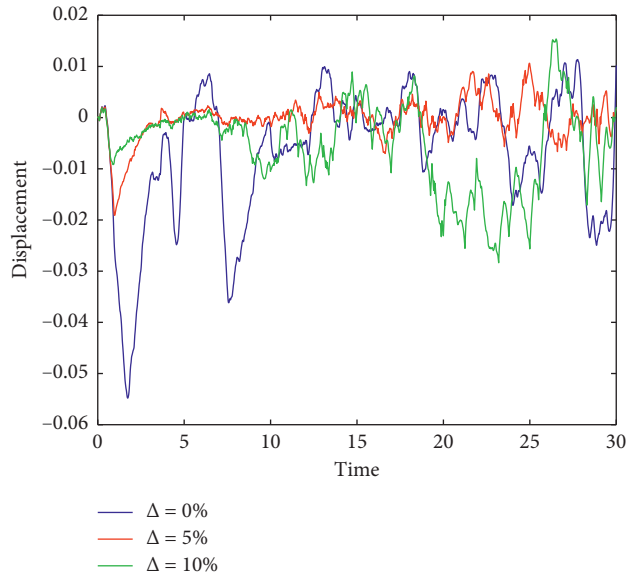

Figure 16: The variations of horizontal displacement of 11th story for the active system and different values of Δ.

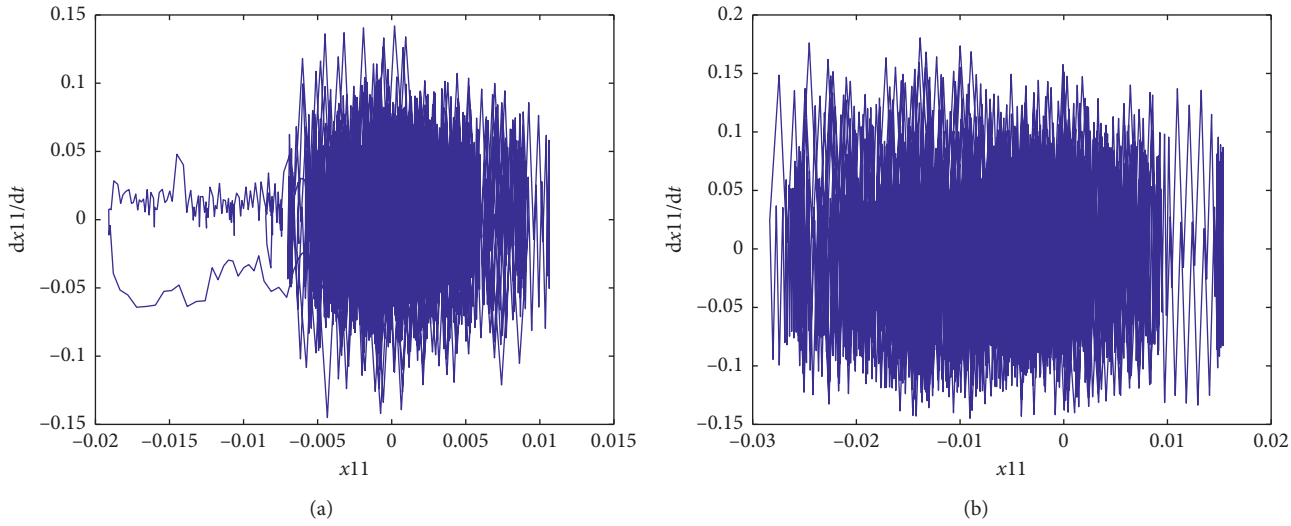

Figure 17: The region of the attraction set for Figure 16 and considering different values of Δ = 5% and Δ = 10%. (a) The region of the attraction set for Δ = 5%. (b) The region of the attraction set for Δ = 10%.

horizontal displacement of the system to increase substantially.

Additionally, the region of attraction for an η value of 100,000 is shown in Figure 13. As shown, the region of attraction is considerably expanded at this η value.

The displacement amplitude of the system for different λ values and a fixed η value of 1 is demonstrated in Figure 14. As shown, the displacement amplitude is substantially decreased by increasing lambda. The region of attraction for a λ value of 5 is shown in Figure 15. Consider this figure suggests that the region of attraction becomes more limited for a lambda value of 5.

This section discusses the controller robustness to system uncertainty. In the first scenario, only the system uncertainties were considered and the actuator uncertainties were neglected. The variations of horizontal displacement for different Δ values are demonstrated in Figure 16. As shown, the controller is highly robust to uncertainties and even within some time intervals, and the horizontal displacement of the system is decreased by increasing Δ.

This is due to the fact that $F(x,t)$ is also increased by increasing Δ. However, as expressed in equation (22), presence of $F(x,t)$ in this equation virtually increases the term $\psi(x,t)+\eta$, and as shown in Figure 12, increasing η increases the controller robustness. The regions of attraction for Δ = 5% and Δ = 10% are plotted in Figure 17. As shown, despite its larger extent for Δ = 10% compared to Δ = 5%, the region of attraction has become more compact.

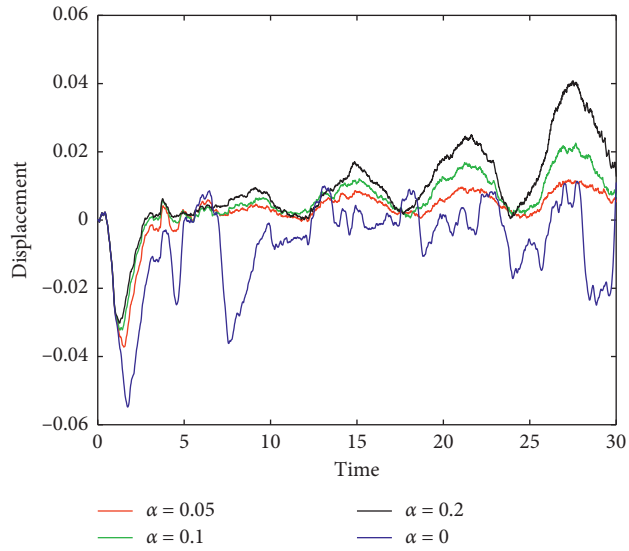

Figure 18: The horizontal displacement of 11^{th} story for the active system considering uncertainty with $\Delta = 1\%$ and different values of α.

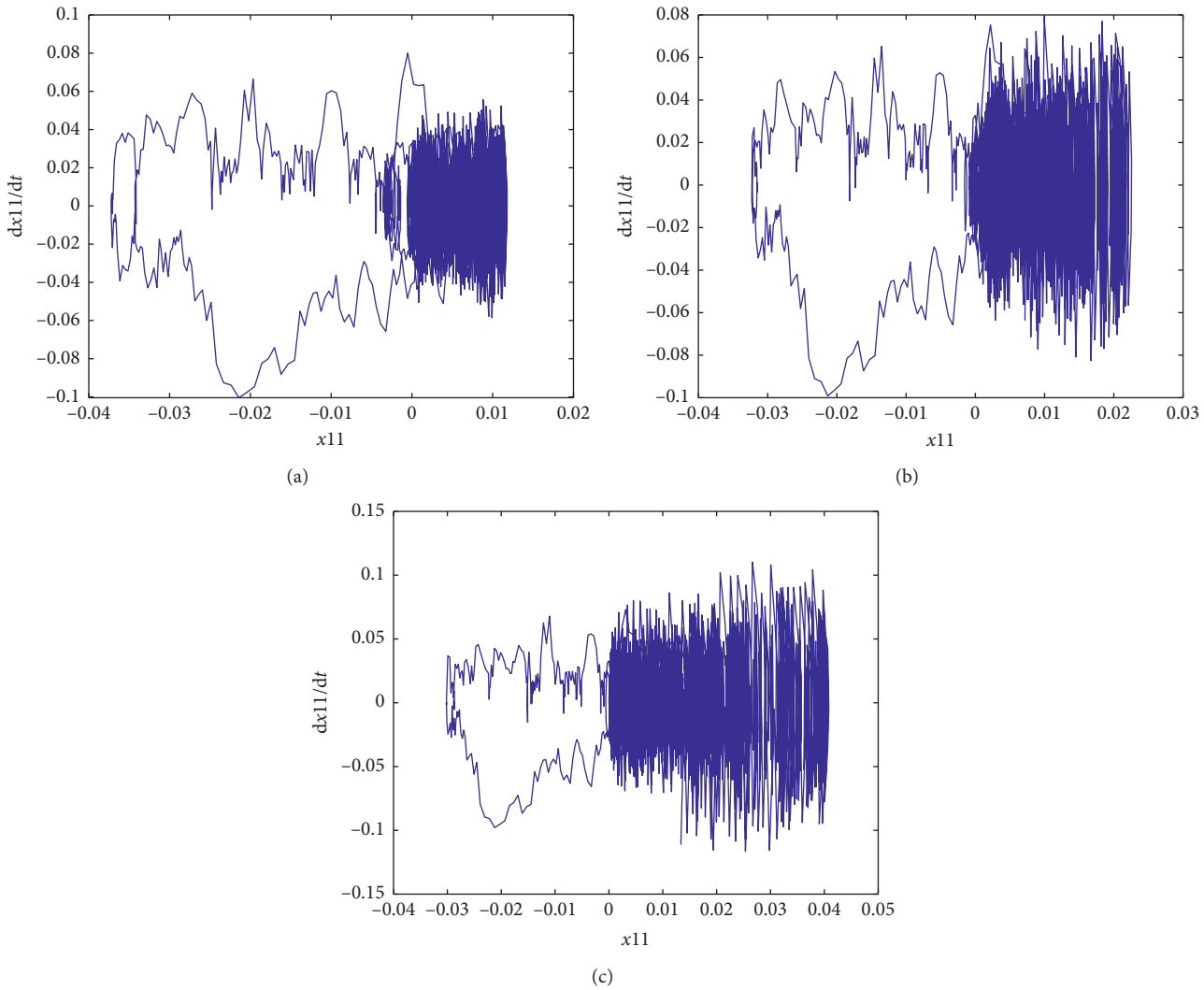

Figure 19: Related phase portrait to Figure 18. (a) $\alpha = 0.05$. (b) $\alpha = 0.1$. (c) $\alpha = 0.2$.

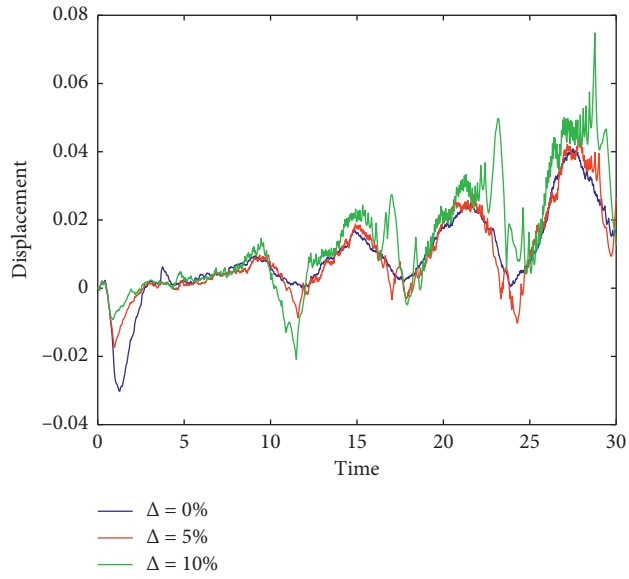

Figure 20: The horizontal displacement of 11^{th} story for the active system considering uncertainty with $\alpha = 0.2$ and different values of Δ. (a) $\Delta = 5\%$. (b) $\Delta = 10\%$.

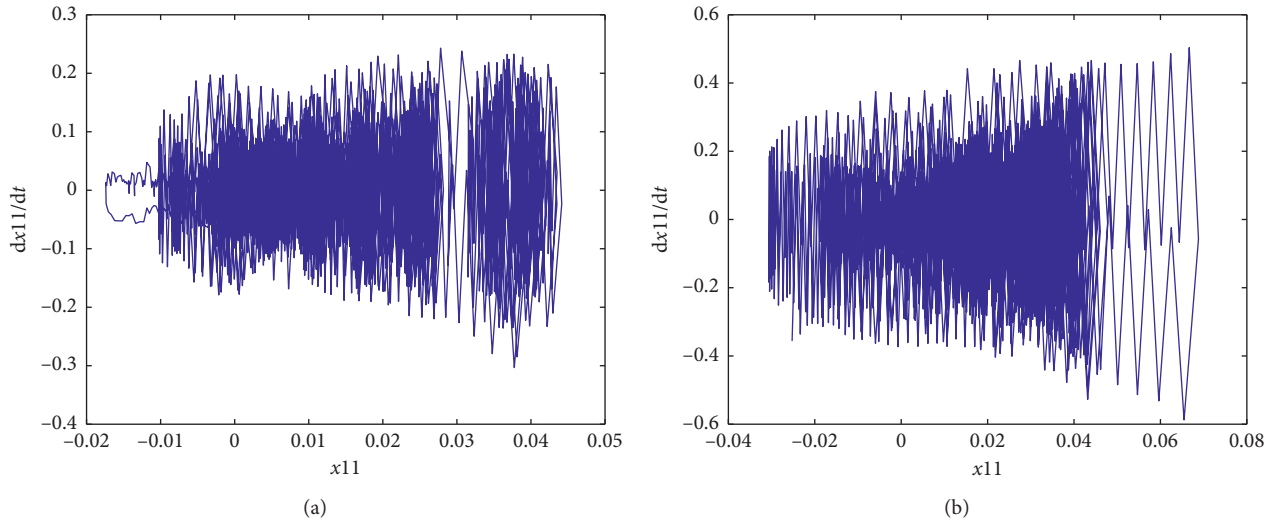

Figure 21: Related phase portrait of Figure 20.

The results for the case with actuator uncertainty and $\Delta = 10\%$ were extracted and presented in Figure 18. In this case, $b(x,t) = 1 + \alpha \sin t$. The results for different α values are shown in this figure, which indicates the significant controller robustness in presence of actuator uncertainty.

The region of attraction in this case is depicted in Figure 19. As shown, the extent of region of attraction is increased by increasing α.

The results in presence of actuator and system uncertainties are shown in Figure 20. In this case, α is set to be 0.2. As shown, the controller exhibits a high robustness in presence of actuator and system uncertainties. The region of attraction for this case is demonstrated in Figure 21. As shown, the extent of region of attraction is increased by increasing Δ.

5. Conclusion

This study has examined the dynamic behavior of an 11-story building equipped with an ATMD system. The stimulation force has been applied on the structure in the form of a Wiener process and an earthquake. The sliding mode scheme has been used to control the ATMD system. So, considering Lipschitz nonlinearity and based on the Ito formulation, a sliding mode controller in the presence of the uncertainty for the general dynamical system with the second-order governing stochastic differential equation has been designed.

The designed controller has been further developed to control the ATMD system. The dynamic behaviors of the

structure in the active and passive modes have been simulated. The presented results demonstrate the high ability of the sliding mode controller to reduce unwanted vibrations of buildings under stimulation of the ground. Also, the results show that the designed controller has a good robustness in the presence of structural and actuator uncertainties. In addition, the effects of the controller parameters on system behavior have been studied. The results show that reduction of ε and increase of η reduce the structural vibration amplitude.

Data Availability

No data were used to support this study.

Conflicts of Interest

The author declares that there are no conflicts of interest.

Acknowledgments

This work was supported by The Research Council of Oman with Grant no. ORG/CBS/14/008.

References

[1] D. Lamberton and B. Lapeyre, *Introduction to Stochastic Calculus Applied to Finance*, Chapman and Hall/CRC, Boca Raton, FL, USA, 2011.

[2] J. M. Steele, *Stochastic Calculus and Financial Applications*, vol. 45, Springer Science & Business Media, Berlin, Germany, 2012.

[3] R. Carmona, *Lectures on BSDEs, Stochastic Control, and Stochastic Differential Games with Financial Applications*, vol. 1, SIAM, Philadelphia, PA, USA, 2016.

[4] B. Remillard, *Statistical Methods for Financial Engineering*, Chapman and Hall/CRC, Boca Raton, FL, USA, 2016.

[5] M. Di Somma, G. Graditi, E. Heydarian-Forushani, M. Shafiekhah, and P. Siano, "Stochastic optimal scheduling of distributed energy resources with renewables considering economic and environmental aspects," *Renewable Energy*, vol. 116, pp. 272–287, 2018.

[6] X. Zhao, T. R. Brown, and W. E. Tyner, "Stochastic techno-economic evaluation of cellulosic biofuel pathways," *Bioresource Technology*, vol. 198, pp. 755–763, 2015.

[7] S. Liu, P. X. Liu, and X. Wang, "Stochastic small-signal stability analysis of grid-connected photovoltaic systems," *IEEE Transactions on Industrial Electronics*, vol. 63, no. 2, pp. 1027–1038, 2015.

[8] N. Onizawa, D. Katagiri, K. Matsumiya, W. J. Gross, and T. Hanyu, "Gabor filter based on stochastic computation," *IEEE Signal Processing Letters*, vol. 22, no. 9, pp. 1224–1228, 2015.

[9] P. Pfeffer, F. Hartmann, S. Höfling, M. Kamp, and L. Worschech, "Logical stochastic resonance with a coulomb-coupled quantum-dot rectifier," *Physical Review Applied*, vol. 4, no. 1, Article ID 014011, 2015.

[10] M. Talha and B. N. Singh, "Stochastic vibration characteristics of finite element modelled functionally gradient plates," *Composite Structures*, vol. 130, pp. 95–106, 2015.

[11] S. Dey, T. Mukhopadhyay, and S. Adhikari, "Stochastic free vibration analyses of composite shallow doubly curved shells–A Kriging model approach," *Composites Part B: Engineering*, vol. 70, pp. 99–112, 2015.

[12] C. Vagg, S. Akehurst, C. J. Brace, and L. Ash, "Stochastic dynamic programming in the real-world control of hybrid electric vehicles," *IEEE Transactions on Control Systems Technology*, vol. 24, no. 3, pp. 853–866, 2015.

[13] J. C. Goodson, B. W. Thomas, and J. W. Ohlmann, "A rollout algorithm framework for heuristic solutions to finite-horizon stochastic dynamic programs," *European Journal of Operational Research*, vol. 258, no. 1, pp. 216–229, 2017.

[14] W. Chai, A. Naess, and B. J. Leira, "Stochastic dynamic analysis and reliability of a vessel rolling in random beam seas," *Journal of Ship Research*, vol. 59, no. 2, pp. 113–131, 2015.

[15] A. Azizi, "Computer-based analysis of the stochastic stability of mechanical structures driven by white and colored noise," *Sustainability*, vol. 10, no. 10, p. 3419, 2018.

[16] A. Azizi and P. G. Yazdi, "Introduction to noise and its applications," in *Computer-Based Analysis of the Stochastic Stability of Mechanical Structures Driven by White and Colored Noise*, Springer, Berlin, Germany, 2019.

[17] A. Azizi and P. G. Yazdi, "Noise control techniques," in *Computer-Based Analysis of the Stochastic Stability of Mechanical Structures Driven by White and Colored Noise*, Springer, Berlin, Germany, 2019.

[18] A. Azizi and P. G. Yazdi, "Mechanical structures: mathematical modeling," in *Computer-Based Analysis of the Stochastic Stability of Mechanical Structures Driven by White and Colored Noise*, Springer, Berlin, Germany, 2019.

[19] A. Azizi and P. G. Yazdi, "White noise: applications and mathematical modeling," in *Computer-Based Analysis of the Stochastic Stability of Mechanical Structures Driven by White and Colored Noise*, Springer, Berlin, Germany, 2019.

[20] A. Azizi and P. G. Yazdi, "Modeling and control of the effect of the noise on the mechanical structures," in *Computer-Based Analysis of the Stochastic Stability of Mechanical Structures Driven by White and Colored Noise*, Springer, Berlin, Germany, 2019.

[21] A. Preciado, A. Orduña, G. Bartoli, and H. Budelmann, "Façade seismic failure simulation of an old cathedral in colima, Mexico by 3D limit analysis and nonlinear finite element method," *Engineering Failure Analysis*, vol. 49, pp. 20–30, 2015.

[22] B. Sołtysik and R. Jankowski, "Building damage due to structural pounding during earthquakes," *Journal of Physics: Conference Series*, vol. 628, 2015.

[23] A. Kumar, D. Choudhury, and R. Katzenbach, "Effect of earthquake on combined pile–raft foundation," *International Journal of Geomechanics*, vol. 16, no. 5, Article ID 04016013, 2016.

[24] K.-S. Park and S.-Y. Ok, "Modal-space reference-model-tracking fuzzy control of earthquake excited structures," *Journal of Sound and Vibration*, vol. 334, pp. 136–150, 2015.

[25] M. Domaneschi and L. Martinelli, "Earthquake-resilience-based control solutions for the extended benchmark cable-stayed bridge," *Journal of Structural Engineering*, vol. 142, no. 8, Article ID C4015009, 2015.

[26] R. Mitchell, Y.-J. Cha, Y. Kim, and A. A. Mahajan, "Active control of highway bridges subject to a variety of earthquake loads," *Earthquake Engineering and Engineering Vibration*, vol. 14, no. 2, pp. 253–263, 2015.

[27] A. Y. Grinberger and D. Felsenstein, *A Tale of Two Earthquakes: Dynamic Agent-Based Simulation of Urban Resilience*, The Hebrew University of Jerusalem, Jerusalem, Israel, 2017.

[28] F. C. Klebaner, *Introduction to Stochastic Calculus with Applications*, World Scientific Publishing Company, Singapore, 2012.
[29] M. Jeanblanc, M. Yor, and M. Chesney, *Mathematical Methods for Financial Markets*, Springer Science & Business Media, Berlin, Germany, 2009.
[30] L. C. G. Rogers and D. Williams, *Diffusions, Markov Processes and Martingales: Volume 2, Itô Calculus*, vol. 2, Cambridge University Press, Cambridge, UK, 2000.
[31] G.-P. Cai, J.-Z. Huang, F. Sun, and C. Wang, "Modified sliding-mode bang-bang control for seismically excited linear structures," *Earthquake Engineering & Structural Dynamics*, vol. 29, no. 11, pp. 1647–1657, 2000.
[32] B. Oksendal, *Stochastic Differential Equations: An Introduction with Applications*, Springer Science & Business Media, Berlin, Germany, 2013.
[33] H. Salarieh and A. Alasty, "Control of stochastic chaos using sliding mode method," *Journal of Computational and Applied Mathematics*, vol. 225, no. 1, pp. 135–145, 2009.
[34] W. S. Levine, *The Control Systems Handbook: Control System Advanced Methods*, CRC Press, Boca Raton, FL, USA, 2018.